

Massive, Absorption-selected Galaxies at Intermediate Redshifts

N. KANEKAR,^{1,*} J. X. PROCHASKA,² L. CHRISTENSEN,³ N. H. P. RHODIN,³ M. NEELEMAN,^{2,4} M. A. ZWAAN,⁵ P. MØLLER,⁵
M. DESSAUGES-ZAVADSKY,⁶ J. P. U. FYNBO,⁷ AND T. ZAFAR⁸

¹*National Centre for Radio Astrophysics, Tata Institute of Fundamental Research, Pune University, Pune 411007, India*

²*University of California Observatories-Lick Observatory, University of California, Santa Cruz, CA, 95064, USA*

³*Dark Cosmology Centre, Niels Bohr Institute, Copenhagen University, Juliane Maries Vej 30, 2100 Copenhagen O, Denmark*

⁴*Max-Planck-Institut für Astronomie, Königstuhl 17, D-69117 Heidelberg, Germany*

⁵*European Southern Observatory, Karl-Schwarzschildstrasse 2, 85748 Garching Bei Muenchen, Germany*

⁶*Observatoire de Genève, Université de Genève, 51 Ch. des Maillettes, 1290 Sauverny, Switzerland*

⁷*The Cosmic Dawn Center, Niels Bohr Institute, Copenhagen University, DK-2100 Copenhagen, Denmark*

⁸*Australian Astronomical Observatory, PO Box 915, North Ryde, NSW 1670, Australia*

ABSTRACT

The nature of absorption-selected galaxies and their connection to the general galaxy population have been open issues for more than three decades, with little information available on their gas properties. Here we show, using detections of carbon monoxide (CO) emission with the Atacama Large Millimeter/submillimeter Array (ALMA), that five of seven high-metallicity, absorption-selected galaxies at intermediate redshifts, $z \approx 0.5 - 0.8$, have large molecular gas masses, $M_{\text{Mol}} \approx (0.6 - 8.2) \times 10^{10} M_{\odot}$ and high molecular gas fractions ($f_{\text{Mol}} \equiv M_{\text{Mol}}/(M_{*} + M_{\text{Mol}}) \approx 0.29 - 0.87$). Their modest star formation rates (SFRs), $\approx (0.3 - 9.5) M_{\odot} \text{ yr}^{-1}$, then imply long gas depletion timescales, $\approx (3 - 120) \text{ Gyr}$. The high-metallicity absorption-selected galaxies at $z \approx 0.5 - 0.8$ appear distinct from populations of star-forming galaxies at both $z \approx 1.3 - 2.5$, during the peak of star formation activity in the Universe, and lower redshifts, $z \lesssim 0.05$. Their relatively low SFRs, despite the large molecular gas reservoirs, may indicate a transition in the nature of star formation at intermediate redshifts, $z \approx 0.7$.

Keywords: galaxies: high-redshift — quasars: absorption lines — ISM: molecules

1. INTRODUCTION

At cosmological distances, galaxies are usually identified by their stellar emission, which causes them to appear bright at rest-frame ultraviolet (UV) and optical wavelengths. Such “emission-selected” samples have been used to glean much information on galaxy evolution, including the detection of galaxy populations at high redshifts, $z \approx 10$ (Oesch et al. 2014), the redshift evolution of the cosmic SFR density (Bouwens et al. 2014) and the UV galaxy luminosity function (Bouwens et al. 2015), relations between the stellar mass of a galaxy and its SFR and metallicity (Tremonti et al. 2004; Noeske et al. 2007), etc. However, such samples, selected in the rest-frame UV or optical, contain an intrinsic bias towards brighter galaxies, and against dusty galaxies (where the dust obscures the optical or UV emission).

An alternative way of identifying high-redshift galaxies, free from this luminosity bias, is to select them based on their absorption signatures in the spectra of higher-redshift quasi-stellar objects (QSOs). The highest HI column density absorption systems ($N_{\text{HI}} \geq 2 \times 10^{20} \text{ cm}^{-2}$), the damped Lyman- α absorbers (DLAs; Wolfe et al. 2005), have long been identified with galaxies at high redshifts, because their HI column densities are similar to those of galaxies in the local Universe and their metallicities are higher than those in the intergalactic medium, indicating enrichment via star formation (Wolfe et al. 2005). Recent searches through the Sloan Digital Sky Survey have revealed more than 10,000 DLAs at $z \gtrsim 2$ (Noterdaeme et al. 2012).

Characterizing the galaxies that give rise to DLAs and connecting them to the emission-selected galaxy population is of great value in studies of galaxy evolution. Absorption studies of DLAs have yielded detailed information about the pencil

Table 1. The results.

QSO	z_{QSO}	z_{abs}^a	N_{HI} $\times 10^{20} \text{ cm}^{-2}$	Beam ^b " × "	RMS _{CO} ^c μJy	$\int S_{\text{CO}} dV^d$ Jy km/s	W20 ^e km/s	$L'_{\text{CO}(1-0)}^f$ $\times 10^9 \text{ K km/s pc}^2$
B0827+243	0.941	0.5247	2.0	2.1×1.6	275	3.11 ± 0.16	425	19.06 ± 0.98
B1629+120	1.795	0.5313	5.0	2.7×2.4	200	0.243 ± 0.040	350	1.53 ± 0.25
J0058+0155	1.954	0.6125	1.1	2.9×2.0	155	< 0.089	–	< 0.75
J2335+1501	0.791	0.6798	0.5	2.7×2.5	185	0.601 ± 0.064	350	6.26 ± 0.67
J1323-0021	1.392	0.7163	3.5	2.7×2.2	175	0.50 ± 0.05	650	5.79 ± 0.58
J1436-0051	1.275	0.7377	1.2	2.8×2.2	150	1.480 ± 0.055	350	18.19 ± 0.68
J0138-0005	1.341	0.7821	0.65	2.9×2.1	155	< 0.082	–	< 1.1

^a The absorber redshift, from low-ionization metal lines.

^b The full-width-at-half-maximum of the ALMA synthesized beam.

^c The root-mean-square (RMS) noise, on the final spectral cube, at a velocity resolution of 100 km/s.

^d The velocity-integrated CO(2–1) line flux density, or the 3σ upper limit on this quantity for the two CO non-detections, assuming a CO line FWHM of 300 km/s.

^e The velocity width of the CO(2–1) line between points that are 20% of the maximum value, for the CO detections (uncorrected for galaxy inclination).

^f The inferred CO(1–0) line luminosity.

beam traced by the QSO sightline, including the metallicity (Rafelski et al. 2012), kinematics (Prochaska & Wolfe 1997), gas temperature (Kanekar et al. 2014), and star formation history (Dessauges-Zavadsky et al. 2007). However, despite many searches, a combination of the bright background QSO and the intrinsic faintness of most high- z DLA hosts has made it hard to detect the stellar emission from the galaxies associated with DLAs at high redshifts, $z \gtrsim 2$ (e.g. Fynbo et al. 2013; Fumagalli et al. 2015; Krogager et al. 2017). At intermediate redshifts, $z \approx 0.5 - 1$, optical attempts to identify the DLA hosts have been more successful, and suggest that the absorbers probe gas in and around star-forming, field galaxies (e.g. le Brun et al. 1997; Rao et al. 2003; Chen et al. 2005).

Until recently, we have had no information on a vital part of the puzzle, the molecular gas in the DLA galaxies that gives rise to star formation. The advent of ALMA has changed the field, with the detections of CO emission from galaxies associated with a $z \approx 0.101$ sub-DLA (Neeleman et al. 2016), a $z \approx 0.7163$ DLA (Møller et al. 2018), a $z \approx 0.633$ Lyman-limit absorber (Klitsch et al. 2018), and a $z \approx 2.193$ DLA (Neeleman et al. 2018), and of the $157.74\mu\text{m}$ fine-structure transition of singly-ionized carbon from galaxies associated with two DLAs at $z \approx 4$ (Neeleman et al. 2017). Neeleman et al. (2016) found the host of the $z = 0.101$ sub-DLA to be a molecule-rich, rotating disk, while Møller et al. (2018) found the galaxy associated with the $z = 0.7163$ DLA to be a massive, molecule-rich galaxy, but with a low SFR. We report here on an ALMA search for redshifted CO(2–1) emission from a sample of seven absorption-selected galaxies at $z \approx 0.5 - 0.8$, selected from known DLAs and sub-DLAs at these redshifts (Rao et al. 2006) based on their high metallicity, $\approx 0.5 - 1.5$ times the solar metallicity. All our targets have galaxies identified at the absorption redshift and close to the quasar sightline, with impact parameter $\lesssim 50$ kpc (Chen et al. 2005; Christensen et al. 2014; Straka et al. 2016; Møller et al. 2018).¹

2. OBSERVATIONS AND DATA ANALYSIS

The Atacama Millimeter/sub-millimeter Array (ALMA) was used to observe the seven target absorbers over 2014 December to 2017 January (programme ID's 2013.1.01178.S and 2015.1.00561.S), using the ALMA Band-4 receivers. All observations used four ALMA 1.875 GHz bands, with one band (sub-divided into 480 channels, using the FDM mode of the correlator) covering the expected redshifted CO(2–1) line frequency, and the other three bands (sub-divided into 128 channels, using the TDM mode) placed at neighbouring frequencies to measure the continuum emission. This yielded a velocity resolution of ≈ 8 km/s for the band covering the redshifted CO(2–1) line, and a total velocity coverage of ≈ 4000 km/s.

The initial calibration of all data was done by the ALMA support staff, using the ALMA data pipeline in the Common Astronomy Software Applications (CASA) package (McMullin et al. 2007). In two cases (B1629+120 and B0827+243), the quasar was sufficiently bright to allow us to self-calibrate the continuum data, which was carried out in the Astronomical Image Processing

¹ We use a flat Λ cold dark matter cosmology throughout this paper, defined by the parameters, $\Omega_{\Lambda} = 0.69$, $\Omega_{\text{M}} = 0.31$ and $H_0 = 71 \text{ km s}^{-1}$ (Ade et al. 2016).

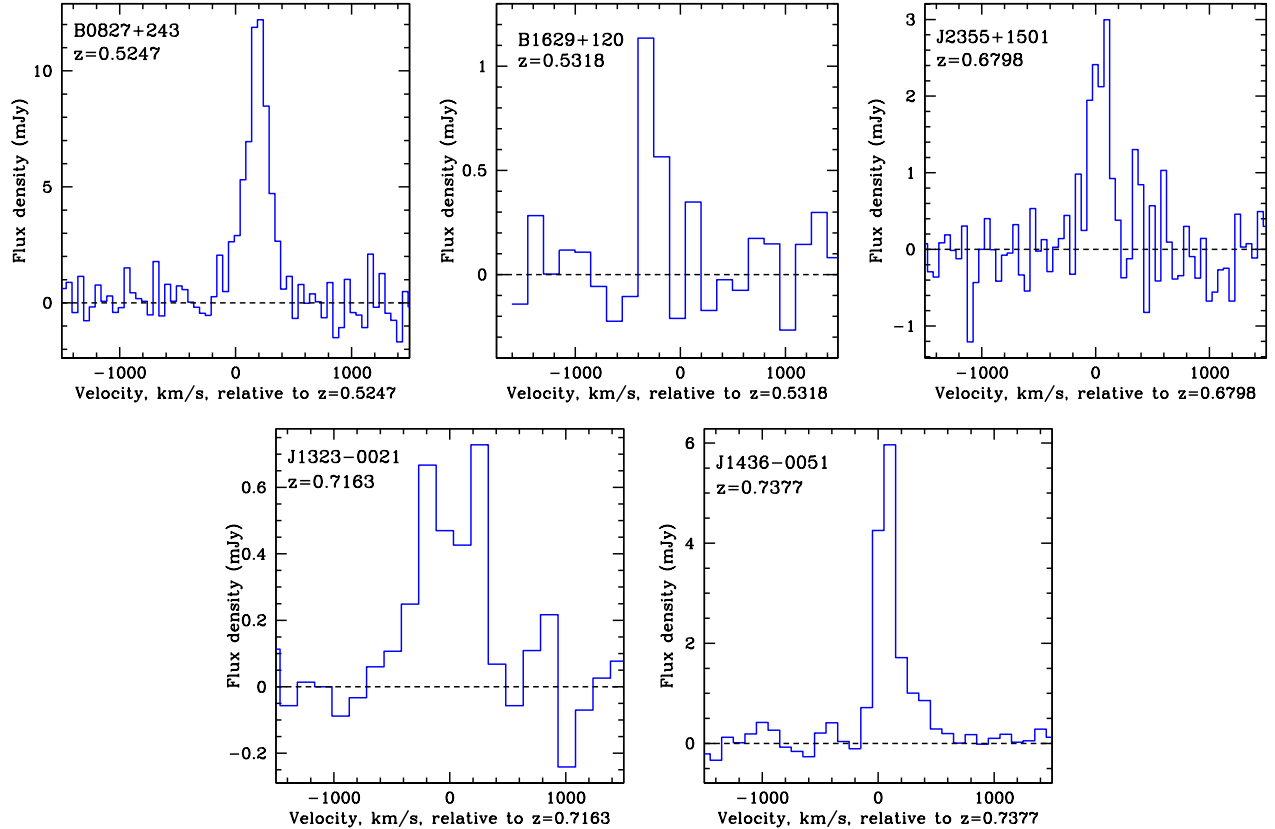


Figure 1. CO(2–1) line spectra for the five detections. The quasar name and the DLA redshift, from low-ionization metal lines, are indicated at the top left corner of each panel. The abscissa shows velocity relative to the absorption redshift. The spectra have been binned into 50 km/s (B0827+243, J2335+1501), 100 km/s (J1436–0051) and 150 km/s (B1629+120, J1323–0021) channels.

System (Greisen 2003). The root-mean-square (RMS) noise on the continuum images was $\approx 13 - 20 \mu\text{Jy}$, except for the field of B0827+243, where the RMS noise was higher ($\approx 40 \mu\text{Jy}$), probably due to dynamic range limitations, as the quasar is very bright, with a flux density of $\approx 568 \text{ mJy}$ at the observing frequency. The antenna-based gains obtained from the procedure were then applied to the CO(2–1) line data, and the continuum image subtracted out to produce a residual visibility data set. This was then imaged in the CASA package to produce the final spectral cubes. The cubes were made at velocity resolutions of 50 – 300 km/s, and used natural weighting, to maximize the signal-to-noise ratio. A correction for the ALMA primary beam was applied to the cubes, before carrying out the search for redshifted CO(2–1) emission.

Redshifted CO(2–1) line emission was detected in five of our seven target fields (see Table 1); the final CO spectra were obtained by measuring the flux density per channel in an elliptical region chosen to contain all detected emission. The $z = 0.7163$ DLA towards J1323–0021 was the only system detected in its rest-frame 230 GHz continuum emission, at $\approx 3.2\sigma$ significance with a flux density of $53 \mu\text{Jy}$; this system is discussed in detail in Møller et al. (2018).

Our ALMA observations detect strong ($> 6\sigma$ significance) redshifted CO(2–1) emission from five of our seven targets, spatially coincident with the optically-identified galaxies and at the galaxy redshift. Fig. 1 shows the CO(2–1) emission line profiles for the five detections, in order of increasing redshift. The CO lines have full-widths-between-20%-points, W_{20} , $\approx 350 - 650 \text{ km s}^{-1}$, similar to widths observed in nearby galaxies (e.g. Saintonge et al. 2011a). Fig. 2 shows the velocity-integrated CO(2–1) emission maps for the five detections. The spatial extent of the integrated CO(2–1) emission was measured using the fitter function in the CASA package; the deconvolved sizes are listed in Table 2. In four of the five cases, the exception being the DLA towards B1629+120, the CO emission is marginally resolved by the ALMA synthesized beam, yielding a spatial extent of $\approx 15 \text{ kpc}$.

3. RESULTS AND DISCUSSION

The molecular gas mass of a galaxy can be inferred from its CO(2–1) line luminosity if one knows the CO-to-H₂ conversion factor (α_{CO}) and the nature of the excitation of the J= 2 level (e.g. Bolatto et al. 2013; Carilli & Walter 2013). For high-metallicity

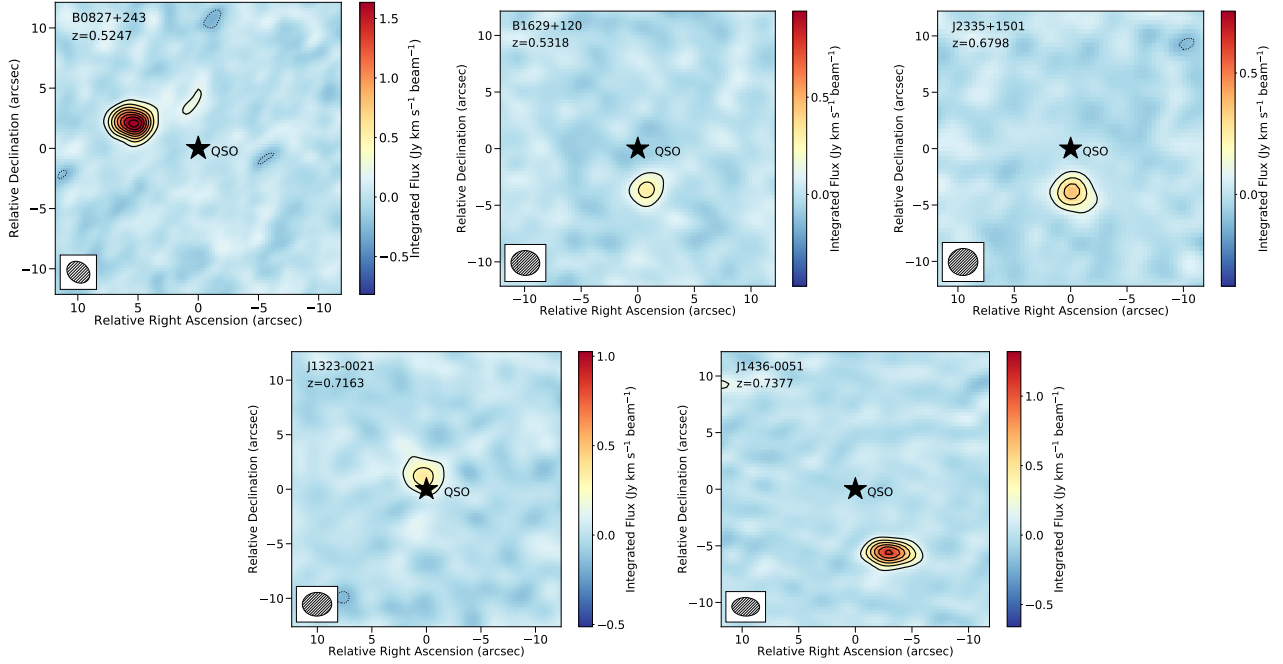


Figure 2. Velocity-integrated CO(2–1) emission for our five detections; the quasar name and the DLA redshift indicated at the top left corner of each panel. The axes co-ordinates are relative to the quasar’s J2000 co-ordinates. The positive (solid) contours are at $(3, 6, 9, \dots) \times \sigma$, and the negative (dashed) contour at -3σ , where σ is the RMS noise on each image. The hatched ellipse in each panel shows the ALMA synthesized beam.

Table 2. The derived properties of the galaxies associated with our seven intermediate-redshift absorbers.

DLA galaxy ^a	z_{abs}^b	M_{mol} $\times 10^9 M_{\odot}$	M_{\star} $\times 10^9 M_{\odot}$	SFR M_{\odot}/yr	f_{Mol}	τ_{dep} Gyr	b^c kpc	Deconvolved angular size
DLA J083052.49+241101.95	0.5247	83.1 ± 4.3	$12.3^{+5.1}_{-3.6}$	0.7 ± 0.1	0.87	119	36.3	$(1.9 \pm 0.2)'' \times (0.85 \pm 0.37)''$
DLA J163145.19+115559.40	0.5313	6.7 ± 1.1	$9.5^{+2.7}_{-0.1}$	1.4 ± 0.1	0.41	4.8	22.8	Unresolved ($< 2.5''$)
DLA J0058+0155	0.6125	< 3.3	$40.7^{+5.0}_{-4.4}$	0.31 ± 0.02	< 0.07	< 11	–	–
DLA J233544.18+150114.47	0.6798	27.3 ± 2.9	$6.8^{+3.1}_{-3.4}$	9.5 ± 0.4	0.80	2.9	26.8	$(1.59 \pm 0.57)'' \times (0.79 \pm 0.57)''$
DLA J132323.82-002153.93	0.7163	25.2 ± 2.5	$63.1^{+24.0}_{-17.4}$	1.6 ± 0.6	0.29	15.7	9.6	$(1.91 \pm 0.21) \times (0.85 \pm 0.37)''$
DLA J143644.85-005156.25	0.7377	79.3 ± 2.9	$25.7^{+6.7}_{-5.3}$	2.2 ± 0.2	0.76	36.7	45.9	$(1.8 \pm 0.2)'' \pm (0.60 \pm 0.21)''$
DLA J0138-0005	0.7821	< 4.9	$7.2^{+1.0}_{-1.0}$	–	< 0.40	–	–	–

^a The galaxy name (“DLA” followed by the J2000 co-ordinates for the CO detections, and “DLA” followed by the QSO’s J2000 co-ordinates for the CO non-detections).

^b The absorber redshift, from low-ionization metal lines.

^c The impact parameter, in kpc, at the absorber redshift, to the quasar line of sight.

galaxies, like spiral disks and starbursts, the CO-to-H₂ conversion factor is typically low, $\alpha_{\text{CO}} \approx 4.36 M_{\odot} (\text{K km/s pc}^2)^{-1}$ (spirals) and $\approx 1 M_{\odot} (\text{K km/s pc}^2)^{-1}$ (starbursts) (Bolatto et al. 2013). To allow for a direct comparison with emission-selected galaxies in the local Universe (the *COLD GASS* sample; e.g. Saintonge et al. 2011a) and at high redshifts (the *PHIBSS* sample; e.g. Tacconi et al. 2013), we will throughout use $\alpha_{\text{CO}} \approx 4.36 M_{\odot} (\text{K km/s pc}^2)^{-1}$. For the line excitation, we assume sub-thermal excitation of the CO $J=2$ level, as is typical in normal spiral galaxies in the local Universe and colour-selected galaxies at high redshifts. In the Milky Way and nearby spirals, the $J=2-1$ line is ≈ 2.5 times stronger than the $J=1-0$ line (e.g. Fixsen et al. 1999; Weiß et al. 2005); we will assume this value for the ratio of the line flux densities in order to infer the CO(1–0) line luminosity, $L'_{\text{CO}(1-0)}$. The inferred molecular gas masses for the galaxies associated with the five absorbers with CO(2–1) line detections lie in the range $(0.6 - 8) \times 10^{10} \times (\alpha_{\text{CO}}/4.36) \times (0.63/r_{21}) M_{\odot}$.

The stellar mass (M_*) of the galaxies associated with six of our seven targets was estimated by fixing the redshift to the spectroscopic value, and matching spectral energy distribution (SED) templates to multi-band photometry using `HyperZ` (Bolzonella et al. 2000) and `LePhare` (Arnouts et al. 1999; Ilbert et al. 2006). We use standard BC03 single stellar population spectral templates (Bruzual & Charlot 2003), assuming a Chabrier initial mass function. M_* is determined by the parameter-set that minimises the χ^2 -statistic across a user pre-defined grid of models. The grid encompasses ages and e-folding time-scales in the ranges 0.01-13.5 Gyrs and 0.1-30 Gyrs respectively, and accounts for intrinsic extinction assuming a standard LMC-Fitzpatrick law. To parametrize the amount of extinction, `HyperZ` accepts reddening as a free parameter, which we vary in the range $A_V = 0 - 1$ mag, whereas `LePhare` accepts a set of user-defined E_{B-V} values, which we select to be in the range 0 - 1. We have verified that `HyperZ` and `LePhare` produce consistent stellar mass estimates, within the uncertainties. We obtain stellar masses in the range $M_* \approx (0.7 - 6.5) \times 10^{10} M_\odot$, listed in Table 2. Note that the stellar mass of the galaxy associated with the $z = 0.7821$ sub-DLA towards J0138-0005 is based on a conversion from its K-band magnitude to the stellar mass (Cappellari et al. 2013).

Finally, the star formation rates (SFRs) of the DLA galaxies were inferred from either the $[\text{OII}]\lambda 3727\text{\AA}$ or $\text{H}\beta\lambda 4382\text{\AA}$ lines (from the literature; e.g. Chen et al. 2005; Christensen et al. 2014; Straka et al. 2016; Møller et al. 2018; Rhodin et al. 2018), or (in the case of the DLA towards B1629+120), from the U -band continuum (Rao et al. 2003), using standard SFR calibrations (Kennicutt & Evans 2012). We do not have an estimate of the SFR for the galaxy associated with the $z = 0.7821$ sub-DLA towards J0138-0005. While these tracers may under-estimate the SFR for dusty galaxies, they allow a fair comparison to the emission-selected samples, where the SFR estimates are based on the $[\text{OII}]\lambda 3727\text{\AA}$ or $\text{H}\alpha\lambda 6563\text{\AA}$ emission line luminosity. The SFRs are relatively low, $\approx (0.3 - 9.5) M_\odot \text{ yr}^{-1}$, again tabulated in Table 2.

The two absorbers with non-detections of CO(2-1) emission, at $z = 0.6125$ towards J0058+0155 and $z = 0.7821$ towards J0138-0005 do not stand out in their absorption properties from the rest of the sample. We note, in passing, that the galaxy counterpart of the $z = 0.7821$ sub-DLA does not have a spectroscopic redshift, while the SFR of the $z = 0.6125$ sub-DLA is the lowest in our sample ($0.31 M_\odot \text{ yr}^{-1}$), despite its relatively high stellar mass ($M_* \approx 4 \times 10^{10} M_\odot$).

Our estimates of the molecular gas mass in the galaxies associated with our seven absorbers allow us to compare the gas properties of high-metallicity, absorption-selected galaxies to those of emission-selected, star-forming galaxies, to test whether the same galaxy populations are being selected by the different methods. Unfortunately, there are few emission-selected galaxies with CO studies at intermediate redshifts, $z \approx 0.7$. For the comparison, we hence used two large emission-selected galaxy samples, the *COLD GASS* sample at low redshifts ($z \lesssim 0.05$), with 212 CO(1-0) detections in galaxies with stellar mass $M_* \geq 10^{10} M_\odot$ (Saintonge et al. 2011a), and the *PHIBSS* sample at high redshifts ($z \approx 1.3, 2.2$) with 49 CO(3-2) detections in galaxies with SFR $\geq 30 M_\odot \text{ yr}^{-1}$ and stellar mass $M_* \geq 2.5 \times 10^{10} M_\odot$ (Tacconi et al. 2013). We assume $\alpha_{\text{CO}} = 4.36 M_\odot (\text{K km s}^{-1} \text{ pc}^2)^{-1}$ for all galaxies.

The four panels of Fig. 3 show comparisons between different properties of the DLA (red), *COLD GASS* (blue) and *PHIBSS* (black) samples. The top-left panel shows the optical properties, with the SFR plotted against the stellar mass: the DLA galaxies appear consistent with being drawn from the population of star-forming galaxies at $z \approx 0.2 - 0.7$ (Noeske et al. 2007) and also with the *COLD GASS* population. The top-right panel plots the molecular gas mass versus the stellar mass: four of the seven DLA galaxies have substantially higher molecular gas masses than the galaxies of the low- z *COLD GASS* sample, at the same stellar masses. The bottom-left panel shows the SFR plotted against the molecular gas mass, with the dashed lines indicating the median molecular gas depletion times ($\tau_{\text{depl}} = M_{\text{Mol}}/\text{SFR}$) for the three samples. The *PHIBSS* and *COLD GASS* galaxies show a clear correlation between SFR and molecular gas mass (Saintonge et al. 2011b; Tacconi et al. 2013), while the DLA galaxies are offset from this correlation, with far lower SFRs at the same molecular gas masses when compared to the *PHIBSS* galaxies, and higher molecular gas masses at the same SFRs, relative to the *COLD GASS* galaxies. The fact that the DLA galaxies lie below the correlation between SFR and molecular gas mass suggests that star formation activity is being quenched in these systems. Consistent with this picture, the median gas depletion time for the DLA galaxies is $\tau_{\text{depl,DLA}} \approx 10$ Gyr, a factor of ≈ 10 larger than the median gas depletion times in the *PHIBSS* and *COLD GASS* samples (≈ 0.7 Gyr and ≈ 1 Gyr, respectively). Finally, the bottom right panel shows the SFR plotted against the molecular gas fraction, $f_{\text{Mol}} = M_{\text{Mol}}/(M_* + M_{\text{Mol}})$: for the *COLD GASS* and *PHIBSS* galaxies, the SFR increases with increasing gas fraction, while the DLA galaxies lie well below this correlation, with substantially lower SFRs at the same molecular gas fraction, or far higher molecular gas fractions at the same SFR.

From Fig. 3, the molecular gas properties of galaxies associated with high-metallicity DLAs at $z \approx 0.7$ appear distinct from those of star-forming galaxies in the local Universe and at high redshift, despite their similar optical properties. The molecular gas masses, gas depletion times, and molecular gas fractions are substantially larger, at the same SFRs, for the absorption-selected galaxies than for the emission-selected galaxies. Our primary selection criterion for the absorption sample, i.e., a high metallicity, allows us to select galaxies similar in stellar mass to those of the *PHIBSS* and *COLD GASS* samples due to the known correlation between metallicity and stellar mass in both star-forming galaxies and DLAs (Tremonti et al. 2004; Møller et al. 2013). Note

that the stellar masses of the DLA galaxies are similar to those of the emission-selected galaxies, with all the DLA galaxies lying within the range of the star-forming main sequence at $z \approx 0.2 - 0.7$ (Noeske et al. 2007).

We have assumed the same CO-to-H₂ conversion factor, $\alpha_{\text{CO}} = 4.36 M_{\odot} (\text{K km s}^{-1} \text{pc}^2)^{-1}$ for all galaxies. A low CO-to-H₂ conversion factor in DLA galaxies, $\alpha_{\text{CO}} \approx 1$, would lower their inferred molecular gas masses, gas fractions, and depletion times by a factor of ≈ 5 , reducing some of the tension between the DLAs and the emission-selected samples. However, such low values of α_{CO} are only seen in starburst galaxies like ultra-luminous infrared galaxies (ULIRGs) (Bolatto et al. 2013). A low α_{CO} value in DLAs would imply that high-metallicity, absorption-selected galaxies at intermediate redshifts are ULIRGs, rather than normal star-forming galaxies. This would be surprising as nothing in the optical images of the DLA galaxies suggests that these are ULIRGs (e.g. Rao et al. 2003; Chen et al. 2005), and it is not clear why the absorption selection should predominantly yield molecule-rich, starburst galaxies. We hence do not consider this possibility to be likely.

The second possibility is that our selection based on high-metallicity absorption indeed picks out typical star-forming galaxies at intermediate redshifts. The normal SFR and stellar mass properties, but distinct molecular gas properties, may then indicate a transition in the nature of star formation, evolving from the large CO reservoirs and high SFRs at the epoch of peak star formation ($z \approx 1 - 3$) to lower SFRs but similarly large molecular masses at $z \approx 0.7$. This might arise if most of the dense molecular gas in these galaxies has been consumed in the process of star formation, and the bulk of the remaining molecular gas is at a low density, insufficient to trigger further star formation (e.g., a “post-starburst” scenario). Such extended diffuse molecular disks would have a large atomic gas cross-section, making them relatively easy to detect in damped Lyman- α absorption. A recent ALMA search for CO emission from two massive post-starburst galaxies at $z \approx 0.7$ with quenched star formation yielded large molecular gas masses, similar to our values (Suess et al. 2017).

While our sample is yet small, our results suggest that high-metallicity galaxies at intermediate redshifts, $z \approx 0.7$, selected via their absorption signatures, have very different molecular gas properties (higher masses, gas fractions, and depletion times) from emission-selected star-forming galaxies both at the peak epoch of star formation in the Universe and at low redshifts, $z < 0.05$. The large inferred molecular gas reservoirs but low levels of star formation suggest that either high-metallicity, absorption-selected galaxies are dusty, starburst systems, or there is a transition in the nature of star formation in galaxies at intermediate redshifts, $z \approx 0.7$.

NK acknowledges support from the Department of Science and Technology via a Swarnajayanti Fellowship (DST/SJF/PSA-01/2012-13). JXP acknowledges support from NSF AST-1412981. LC and NHPR are supported by DFF -4090-00079. Support for this work was provided by the NSF through award SOSPA2-002 from the NRAO. ALMA is a partnership of ESO (representing its member states), NSF (USA) and NINS (Japan), together with NRC (Canada), NSC and ASIAA (Taiwan), and KASI (Republic of Korea), in cooperation with the Republic of Chile. The Joint ALMA Observatory is operated by ESO, AUI/NRAO and NAOJ. The data reported in this paper are available through the ALMA archive (<https://almascience.nrao.edu/alma-data/archive>) with project codes: ADS/JAO.ALMA #2013.1.01178.S and #2015.1.01034.S.

REFERENCES

- Ade, P. A. R., et al. 2016, *A&A*, 594, A13
- Arnouts, S., Cristiani, S., Moscardini, L., Matarrese, S., Lucchin, F., Fontana, A., & Giallongo, E. 1999, *MNRAS*, 310, 540
- Bolatto, A. D., Wolfire, M., & Leroy, A. K. 2013, *ARA&A*, 51, 207
- Bolzonella, M., Miralles, J.-M., & Pelló, R. 2000, *A&A*, 363, 476
- Bouwens, R. J., et al. 2014, *ApJ*, 795, 126
- Bouwens, R. J., et al. 2015, *ApJ*, 803, 34
- Bruzual, G. & Charlot, S. 2003, *MNRAS*, 344, 1000
- Cappellari, M., et al. 2013, *MNRAS*, 432, 1862
- Carilli, C. L. & Walter, F. 2013, *ARA&A*, 51, 106
- Chen, H.-W., Kennicutt, Jr., R. C., & Rauch, M. 2005, *ApJ*, 620, 703
- Christensen, L., Møller, P., Fynbo, J. P. U., & Zafar, T. 2014, *MNRAS*, 445, 225
- Dessauges-Zavadsky, M., Calura, F., Prochaska, J. X., D’Odorico, S., & Matteucci, F. 2007, *A&A*, 470, 431
- Fixsen, D. J., Bennett, C. L., & Mather, J. C. 1999, *ApJ*, 526, 207
- Fumagalli, M., O’Meara, J. M., Prochaska, J. X., Rafelski, M., & Kanekar, N. 2015, *MNRAS*, 446, 3178
- Fynbo, J. P. U., et al. 2013, *MNRAS*, 436, 361
- Greisen, E. W. 2003, in *Astrophysics and Space Science Library*, Vol. 285, *Information Handling in Astronomy - Historical Vistas*, ed. A. Heck, 109
- Ilbert, O., et al. 2006, *A&A*, 457, 841
- Kanekar, N., et al. 2014, *MNRAS*, 438, 2131
- Kennicutt, R. C. & Evans, N. J. 2012, *ARA&A*, 50, 531
- Klitsch, A., Péroux, C., Zwaan, M. A., Smail, I., Oteo, I., Biggs, A. D., Popping, G., & Swinbank, A. M. 2018, *MNRAS*, 475, 492

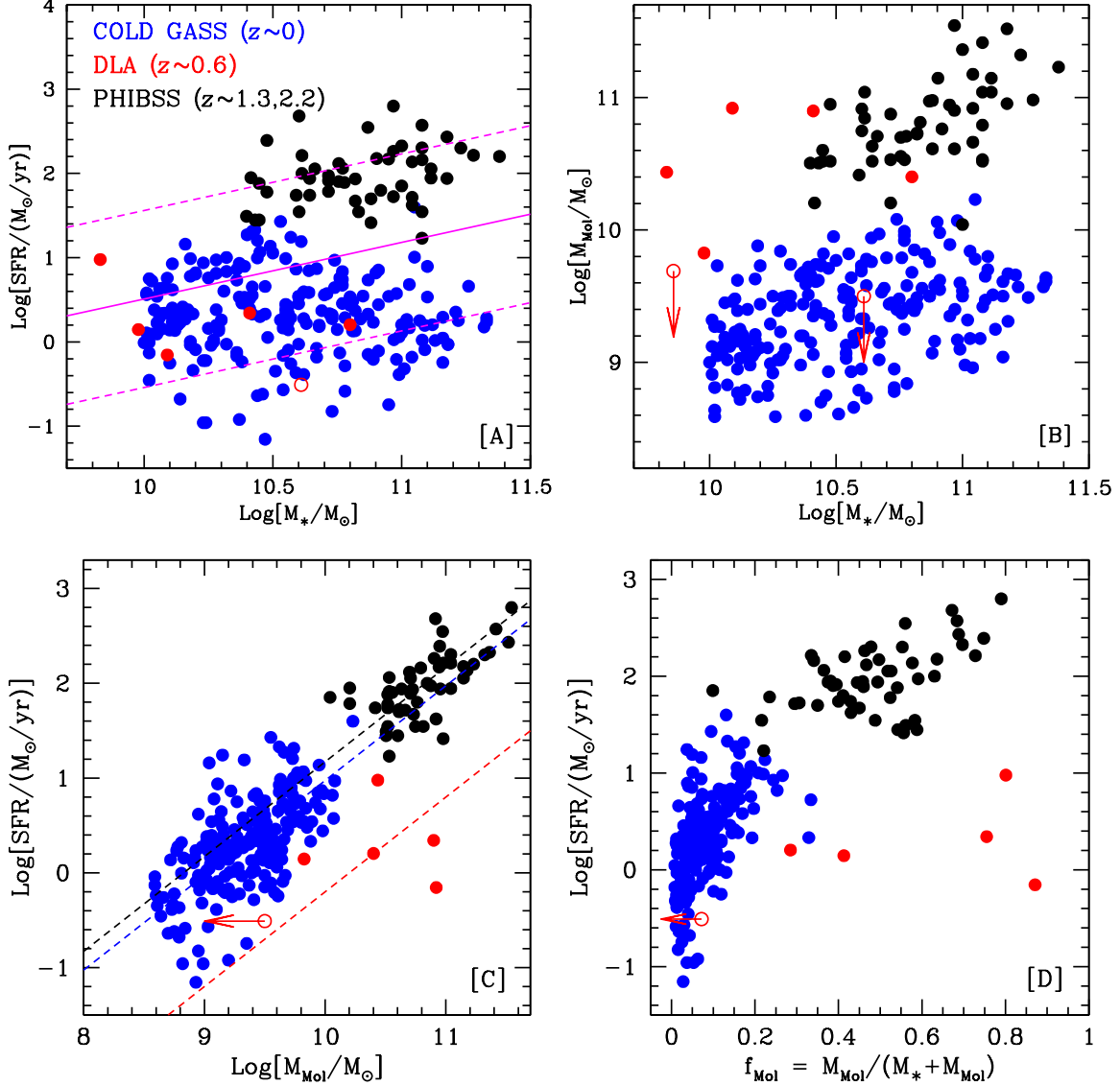


Figure 3. Comparisons between various stellar and gas properties of the galaxies associated with intermediate-redshift absorbers (shown in red) with those of two large emission-selected galaxy samples, the *COLD GASS* sample at $z \approx 0$ (in blue; (Saintonge et al. 2011a)) and the *PHIBSS* sample at $z \approx 1.3, 2.2$ (in black; (Tacconi et al. 2013)). [A] The SFR plotted against the stellar mass: the solid magenta line shows the main-sequence relation of star-forming galaxies at $z \approx 0.2 - 0.7$, with the dashed magenta lines showing the $\pm 3\sigma$ scatter in the relation (Noeske et al. 2007). [B] The molecular gas mass plotted versus the stellar mass. [C] The SFR plotted versus the molecular gas mass; the three dashed lines in the figure indicate the median gas depletion times for the three samples. [D] The SFR plotted versus the molecular gas fraction. See text for discussion.

Krogager, J.-K., Møller, P., Fynbo, J. P. U., & Noterdaeme, P. 2017, *MNRAS*, 469, 2959

le Brun, V., Bergeron, J., Boissé, P., & Deharveng, J.-M. 1997, *A&A*, 321, 733

McMullin, J. P., Waters, B., Schiebel, D., Young, W., & Golap, K. 2007, in *Astronomical Society of the Pacific Conference Series*, Vol. 376, *Astronomical Data Analysis Software and Systems XVI*, ed. R. A. Shaw, F. Hill, & D. J. Bell, 127

Møller, P., Christensen, L., Zwaan, M. A., Kanekar, N., Prochaska, J. X., Rhodin, N. H. P., Dessauges-Zavadsky, M., Fynbo, J. P. U., Neeleman, M., & Zafar, T. 2018, *MNRAS*, 474, 4039

Møller, P., Fynbo, J. P. U., Ledoux, C., & Nilsson, K. K. 2013, *MNRAS*, 430, 2680

Neeleman, M., Kanekar, N., Prochaska, J. X., Christensen, L., Dessauges-Zavadsky, M., Fynbo, J. P. U., Møller, P., & Zwaan, M. A. 2018, *ApJL*, in press (arxiv:1803.05914)

Neeleman, M., Kanekar, N., Prochaska, J. X., Rafelski, M., Carilli, C. L., & Wolfe, A. M. 2017, *Science*, 355, 1285

- Neeleman, M., Prochaska, J. X., Zwaan, M. A., Kanekar, N., Christensen, L., Dessauges-Zavadsky, M., Fynbo, J. P. U., van Kampen, E., Møller, P., & Zafar, T. 2016, *ApJL*, 820, L39
- Noeske, K. G., et al. 2007, *ApJ*, 660, L43
- Noterdaeme, P. et al. 2012, *A&A*, 547, L1
- Oesch, P. A., et al. 2014, *ApJ*, 786, 108
- Prochaska, J. X. & Wolfe, A. M. 1997, *ApJ*, 487, 73
- Rafelski, M., Wolfe, A. M., Prochaska, J. X., Neeleman, M., & Mendez, A. J. 2012, *ApJ*, 755, 89
- Rao, S. M., Nestor, D. B., Turnshek, D. A., Lane, W. M., Monier, E. M., & Bergeron, J. 2003, *ApJ*, 595, 94
- Rao, S. M., Turnshek, D. A., & Nestor, D. B. 2006, *ApJ*, 636, 610
- Rhodin, N. H. P., Christensen, L., Møller, P., Zafar, T., & Fynbo, J. P. U. 2018, *A&A*, submitted
- Saintonge, A., et al. 2011a, *MNRAS*, 415, 32
- Saintonge, A., et al. 2011b, *MNRAS*, 415, 61
- Straka, L. A., Johnson, S., York, D. G., Bowen, D. V., Florian, M., Kulkarni, V. P., Lundgren, B., & Péroux, C. 2016, *MNRAS*, 458, 3760
- Suess, K. A., Bezanson, R., Spilker, J. S., Kriek, M., Greene, J. E., Feldmann, R., Hunt, Q., & Narayanan, D. 2017, *ApJL*, 846, L14
- Tacconi, L. J., et al. 2013, *ApJ*, 768, 74
- Tremonti, C. A., et al. 2004, *ApJ*, 613, 898
- Weiß, A., Downes, D., Walter, F., & Henkel, C. 2005, *A&A*, 440, L45
- Wolfe, A. M., Gawiser, E., & Prochaska, J. X. 2005, *ARA&A*, 43, 861